

Staggered quantum phases of dipolar bosons at finite temperatures

Kuldeep Suthar^{1,*} and Kwai-Kong Ng^{2,†}

¹*Institute of Atomic and Molecular Sciences, Academia Sinica, 10617 Taipei, Taiwan*

²*Department of Applied Physics, Tunghai University, Taichung 40704, Taiwan*

(Dated: November 10, 2022)

The extended Bose-Hubbard model with correlated tunneling exhibits staggered superfluid and supersolid quantum phases. We study finite-temperature phase transitions of quantum phases of dipolar bosons in a two-dimensional optical lattice using mean-field Gutzwiller and quantum Monte Carlo approaches. When nearest-neighbor repulsion is comparable to the on-site interaction, we find that the two topologically distinct superfluids are separated by a normal fluid phase, while at stronger off-site interactions, density-modulated insulating quantum phases appear. We estimate the critical temperature of the staggered superfluid to normal fluid transition and show that this transition is of the Kosterlitz-Thouless type. Finally, we elucidate the coexistence of staggered quantum phases in the presence of an external trapping potential. Our study paves a way to observe novel staggered quantum phases in recent dipolar optical lattice experiments.

I. INTRODUCTION

The ultracold atomic gases trapped in an optical lattice provide a powerful tool to simulate the low-energy behavior of the effective Hamiltonians of condensed matter models [1–4]. Excellent experimental control over the model parameters led to the observation of the Mott insulator (MI) to superfluid (SF) phase transition [5], realization of the Hofstadter model [6], and various novel phenomena in many-body physics [7]. This set-up can also be used to investigate effects that are not possible in conventional solid-state physics, such as tuning the interparticle interaction strength [8] and generating very strong effective magnetic fields [9]. The Bose-Hubbard model (BHM) describes interatomic interactions at a lattice site. However, other interaction processes also affect the properties of strongly-correlated materials. In particular, the bond-charge interaction of the extended Hubbard model [10] has been invoked to explain various phenomena including high-temperature superconductivity [11–13]. Due to the lack of precise control over the interaction strengths, as well as the complexity of materials, interaction-induced phenomena cannot be probed in condensed matter physics.

The unique features of the ultracold atoms and optical lattices create an ideal platform to study complex phenomena due to interparticle particle interactions [4, 14]. For long-range interacting atomic gas, the introduction of nearest-neighbor (NN) interaction induces charge density-wave (CDW) and supersolid (SS) ground states, which spontaneously break the translational symmetry of the lattice [15, 16]. At higher average atomic densities, the onsite interaction results in higher order tunneling processes. One such effect is density-induced tunneling (DIT) which is analogous to the bond-charge interaction of fermions. This considerably affects the properties of soft-core dipolar bosons. Theoretical investigations have shown the influence of DIT on MI-SF quantum phase transitions [17–19], Bose-Fermi multi-component mixtures [20–24], band structures [18], nonequi-

librium dynamics [25], and the emergence of staggered quantum phases [26–29]. The density-induced tunneling has been observed in recent quantum gas experiments [25, 30]. The ramp of the lattice potential and the heating mechanism during time-of-flight measurements contribute to thermal fluctuations in experiments. The excited states in the system affect the parameter region of quantum phases and a normal fluid (NF) state appears in the system at finite temperatures. Several previous studies have discussed the role of finite temperature on the homogeneous system for MI-SF transition of BHM [31–37] and CDW-SS transition of extended BHM [38–40]. Moreover, the effects of the trapping potential on the coexistence of uniform and density-modulated phases are also examined for short- [35, 41, 42] and long-range many-body systems [38, 43, 44]. Since experiments are performed at finite temperatures, it is imperative to consider the role of thermal fluctuations in determining the thermal and insulating regions [45, 46]. Moreover, the effects of finite temperatures on the staggered superfluidity of strongly-correlated quantum many-body systems remain unanswered.

In the present work, we investigate the finite-temperature phase diagram of a homogeneous two-dimensional extended Bose-Hubbard model with correlated hopping. In particular, we focus on higher average number densities where interaction-induced processes lead to staggered quantum phases. Our results show the role of thermal fluctuations resulting in a NF state which intervenes in two different kinds of superfluidity, one due to single-particle hopping while the other is due to DIT. In order to have experimental relevance, we examine both the finite-size effects and the phase coexistence caused by the trapping potential. The thermal phase transition of staggered superfluidity follows the Kosterlitz-Thouless (KT) transition. We discuss the combined effects of trapping and finite-temperature and identify the parameter regime of staggered superfluidity.

The paper is organized as follows. In Sec. II we introduce the model Hamiltonian of isotropic dipolar bosons and describe the approaches used in the present work. We discuss the finite-temperature phase diagrams for weak and strong off-site interactions in the presence of correlated tunneling in Sec. III. In Sec. IV we further examine the finite-size effects of staggered quantum phases using the quantum Monte Carlo

* Corresponding author. kuldeep@gate.sinica.edu.tw

† Corresponding author. kkng@thu.edu.tw

approach. The coexistence of staggered quantum phases at finite temperatures in an external harmonic trapping potential is discussed in Sec. V. Finally, we conclude in Sec. VI.

II. HAMILTONIAN AND METHODS

A. Extended Bose-Hubbard model with correlated hopping

We consider spinless bosons with long-range dipolar interactions in a two-dimensional square optical lattice. The atoms can hop between nearest-neighbor sites of the lattice and experience on-site repulsion. The dipolar interaction considered here is isotropic in nature and as a minimal model, the atoms of nearest-neighboring sites interact repulsively. The model Hamiltonian reads as [30]

$$\hat{H} = -t \sum_{\langle i,j \rangle} \left(\hat{b}_i^\dagger \hat{b}_j + \text{H.c.} \right) + \frac{U}{2} \sum_i \hat{n}_i (\hat{n}_i - 1) + \sum_{\langle i,j \rangle} \left[V \hat{n}_i \hat{n}_j - t' \hat{b}_i^\dagger (\hat{n}_i + \hat{n}_j) \hat{b}_j \right] - \mu \sum_i \hat{n}_i. \quad (1)$$

The bosonic operator \hat{b}_i^\dagger (\hat{b}_i) creates (annihilates) an atom at i th lattice site, and $\hat{n}_i = \hat{b}_i^\dagger \hat{b}_i$ is the corresponding number operator. The first term describes the kinetic energy with t as the hopping strength between nearest-neighbor sites i and j on a square lattice with periodic boundary conditions. The second term represents the on-site repulsive interaction between atoms with strength U . The third term is the long-range interaction which includes the nearest-neighbor repulsive interaction V and density-induced tunneling with strength t' , depending on the density of atoms at each site. The last term μ denotes the chemical potential which controls the atomic density in the grand canonical ensemble.

B. Methods

To study the ground state properties of the system at finite temperatures, we first use the Gutzwiller mean-field approach [47–51]. In the mean-field approximation, the bosonic annihilation operator is decomposed as $\hat{b}_i = \langle \hat{b}_i \rangle + \delta \hat{b}_i$ where $\langle \hat{b}_i \rangle \equiv \phi_i$ is the mean-field, also referred to as the superfluid order parameter, and $\delta \hat{b}_i$ is the fluctuation operator. A similar decomposition for the creation operator can be defined. Using this approximation, the Hamiltonian decouples the sites and all the off-site contributions are incorporated through the mean-field. The many-body Gutzwiller wave function is

$$|\Psi_{\text{GW}}\rangle = \prod_i |\psi_i\rangle = \prod_i \sum_n^{n_{\text{max}}} c_n^i |n_i\rangle, \quad (2)$$

where $|n_i\rangle$ is occupation basis state with n atoms at i th site, and we introduce a cut-off n_{max} on the maximum number of bosons per site, and c_n^i are the complex coefficients for the state $|\psi_i\rangle$. The $|\Psi_{\text{GW}}\rangle$ is normalized by the correspond-

ing complex coefficients c_n^i . At zero temperature, the SF order parameter is a measure of the off-diagonal long-range order or long-range phase coherence $\phi_i \equiv \langle \Psi_{\text{GW}} | \hat{b}_i | \Psi_{\text{GW}} \rangle = \sum_n \sqrt{n} c_{n-1}^* c_n^i$. It is finite for the SF phase while zero for the incompressible phase. The average density ρ is given by $\sum_i n_i / L^2$ where L is the system size. The atomic density at i th lattice site is $n_i \equiv \langle \Psi_{\text{GW}} | \hat{n}_i | \Psi_{\text{GW}} \rangle = \sum_n n |c_n^i|^2$. The density-assisted correlation or DIT order parameter is

$$\eta_i = \langle \Psi_{\text{GW}} | \hat{n}_i \hat{b}_i | \Psi_{\text{GW}} \rangle = \sum_n \sqrt{n} (n-1) c_{n-1}^{*i} c_n^i, \quad (3)$$

which is finite for phases with finite SF order parameter.

At finite temperatures, the presence of thermal fluctuations significantly modifies the phase transitions of the system [38, 52–54]. The order parameters defining the superfluidity and density-dependent transport properties are given by their thermal averages. We retain the entire energy spectrum E_i^l and eigenstates $|\psi\rangle_i^l$ obtained from the diagonalization of mean-field Hamiltonian. Then, the partition function of the system is $Z = \sum_l e^{-\beta E^l}$, where $\beta = (k_B T)^{-1}$ is the inverse of thermal energy at temperature T . The thermal average of the order parameters is

$$\langle \phi_i \rangle = \frac{1}{Z} \sum_l {}_i^l \langle \psi | \hat{b}_i e^{-\beta E^l} | \psi \rangle_i^l, \quad (4a)$$

$$\langle n_i \rangle = \frac{1}{Z} \sum_l {}_i^l \langle \psi | \hat{n}_i \hat{b}_i e^{-\beta E^l} | \psi \rangle_i^l, \quad (4b)$$

where $\langle \dots \rangle$ represents the thermal averaging of the observable. Additionally, the average local occupancy at finite T is defined as

$$\langle \hat{n}_i \rangle = \frac{1}{Z} \sum_l {}_i^l \langle \psi | \hat{n}_i e^{-\beta E^l} | \psi \rangle_i^l, \quad (5)$$

from which the average density at finite T is $\rho = \sum_i \langle \hat{n}_i \rangle / L^2$. The introduction of finite T leads to the appearance of the NF phase. The NF phase is a compressible phase and it can be distinguished from other insulating MI and CDW phases by inspecting the compressibility [35, 45]. The compressibility, which is the measure of local density variance, is $\kappa = \sum_i (\langle \hat{n}_i^2 \rangle - \langle \hat{n}_i \rangle^2) / L^2$. At finite T , due to the presence of thermal fluctuations, the insulating phases appear with nearly integer site occupancy whereas NF phase has real occupancy. Ideally, κ is zero for insulating MI and CDW phases while it is nonzero for the NF phase. In the mean-field approach, the crossover between the insulating MI or CDW phase and NF phase is determined by the value of κ . Here, we identify NF phase by $\kappa > 10^{-5}$ [35, 55] and $\phi = \eta = 0$. The zero SF order parameter also distinguishes NF phase from other compressible phases. Furthermore the single-particle correlation and structure factor which are the measure of off-diagonal and

diagonal long-range order, for momentum wave-vector \mathbf{k} are

$$M(\mathbf{k}) = \frac{1}{L^2} \sum_{j,j'} e^{i\mathbf{k} \cdot (\mathbf{r}_j - \mathbf{r}_{j'})} \langle \hat{b}_j^\dagger \hat{b}_{j'} \rangle, \quad (6a)$$

$$S(\mathbf{k}) = \frac{1}{L^2} \sum_{j,j'} e^{i\mathbf{k} \cdot (\mathbf{r}_j - \mathbf{r}_{j'})} \langle \hat{n}_j \hat{n}_{j'} \rangle. \quad (6b)$$

Complementary to the Gutzwiller mean-field approach, we also employ the quantum Monte Carlo (QMC) method to study the finite temperature phase diagrams of the model. In principle, at finite T , QMC is numerically exact and only subjects to the finite-size effect and statistical error if the infamous sign problem is absent [56]. Unfortunately, in our extended BHM \hat{H} , a negative value of the DIT (t') competes with the single-particle hopping t ($t > 0$) that the overall effective hopping matrix elements,

$$\begin{aligned} \langle n_i + 1, n_j - 1 | -t \hat{b}_i^\dagger \hat{b}_j - t' \hat{b}_i^\dagger (\hat{n}_i + \hat{n}_j) \hat{b}_j | n_i, n_j \rangle & \quad (7) \\ = [-t - t'(n_i + n_j - 1)] \sqrt{n_i + 1} \sqrt{n_j}, \end{aligned}$$

can be either positive or negative, depends on the neighboring local particle densities n_i and n_j . This leads to possible opposite signs in the QMC simulation that cannot be removed with some simple transformation. In that case, the statistical uncertainty tends to diverge at low enough temperatures. Nevertheless, for most of the parameter regime and temperature range we investigate in this work, the average sign is not close to zero, therefore the sign problem is manageable to provide reliable observable measurements.

We adopt the well-established stochastic series expansion approach with a directed loop algorithm to simulate the model Hamiltonian \hat{H} [57, 58]. As usual, the superfluidity is measured via the fluctuation of winding numbers W_x and W_y :

$$\rho_s = \frac{1}{2\beta} (\langle W_x^2 \rangle + \langle W_y^2 \rangle). \quad (8)$$

On the other hand, the computation of the off-diagonal order parameter $M(\mathbf{k})$ requires the measurement of the matrix elements $\langle \hat{b}_j^\dagger \hat{b}_{j'} \rangle$ which can be carried out directly during the loop update [59]. While the compressibility κ is related to the density variance, which in turn is affected by the average sign of each measurement, it is problematic to calculate κ when opposite signs arise in the simulation. Therefore in our QMC calculations, instead of measuring the compressibility κ , we identify the boundary between the MI and NF phases by observing the saturation of the particle occupancy as temperature is reduced. In general, we restrict the maximum particle occupancy up to 6 and set the lattice size $L = 36$.

III. FINITE-TEMPERATURE PHASE DIAGRAMS

The competition between various terms in the model Hamiltonian leads to different phases at zero temperature. For $V = t' = 0$, the competitions between the kinetic and on-site interaction energy leads to two quantum phases of BHM [60, 61]. Most of the phase diagram consists of

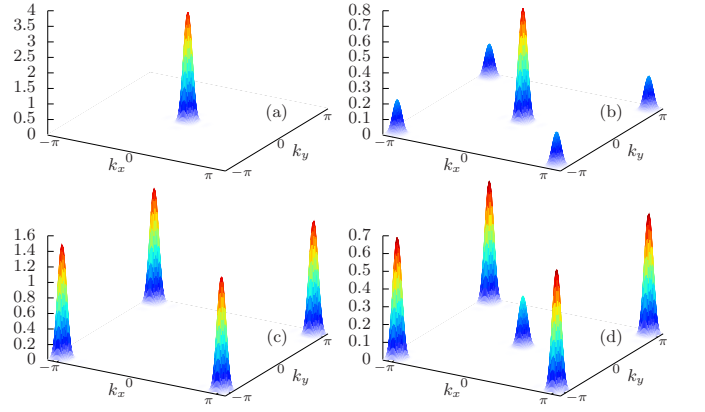


FIG. 1. Examples of the momentum distributions of $M(\mathbf{k})$ for the compressible phases of dipolar bosons in two-dimensional optical lattices. (a) SF phase: the off-diagonal long-range order associated with superfluidity results in a sharp peak in $M(\mathbf{k})$ at the center of the Brillouin zone. (b) SS phase: the nearest-neighbor interaction leads to a supersolid compressible phase which exhibits a sharp peak in $M(\mathbf{k})$ at the center (due to the superfluid nature) and smaller peaks at the corners of the Brillouin zone (due to the long-range diagonal order). (c,d) SSF and SSS phases: in both cases the largest peaks move to the corners of the Brillouin zone.

Bose-Einstein condensed superfluid phase which possesses off-diagonal long-range order and is phase coherent. The momentum distribution of the single-particle correlation $M(\mathbf{k})$ for SF phase is shown in Fig. 1(a) which shows a sharp peak of $M(\mathbf{k})$ at $\mathbf{k} = (0, 0)$. This indicates a finite superfluid stiffness (or SF order parameter) $\rho_s \neq 0$ ($\phi \neq 0$). For integer mean atomic densities and strong repulsion, the Mott insulator phase appears in the lobe structures in $t - \mu$ plane of a homogeneous system. The size of the insulating lobes decreases with increasing μ as the corresponding larger mean-density favors superfluidity in the system. The MI phase is an incompressible phase with $M(\mathbf{k}) = \rho_s = 0$. At finite temperatures, the interplay of the quantum and thermal fluctuations results into a third, NF phase [32, 35, 62–64]. This phase has zero ρ_s even though the local atomic occupancy is incommensurate. In the finite-temperature phase diagrams, there is no broken symmetry between the insulating and NF phases, hence the transition across these phases exhibit a smooth crossover which is signaled by the change in the compressibility. Around the tip of the lobes, due to prevailing role of quantum fluctuations, the mean-field and quantum Monte Carlo approaches predict different phases [45, 65]. This is due to the limitation of the mean-field theory, in which once the SF order parameter ϕ is zero, the hopping terms do not play any role. And, this underestimate the temperature-induced NF state around the tips of the insulating lobes.

The introduction of an off-site nearest neighbor interaction $V \neq 0$ offers to stabilize quantum phases with spatial ordering, which is identified by the structure factor at finite momentum, for example for checkerboard compressible phases $S(\pi, \pi) \neq 0$. This leads to two new phases, charge-density wave solid phase with integer or half-integer mean-densities, and supersolid phase which breaks two continuous symme-

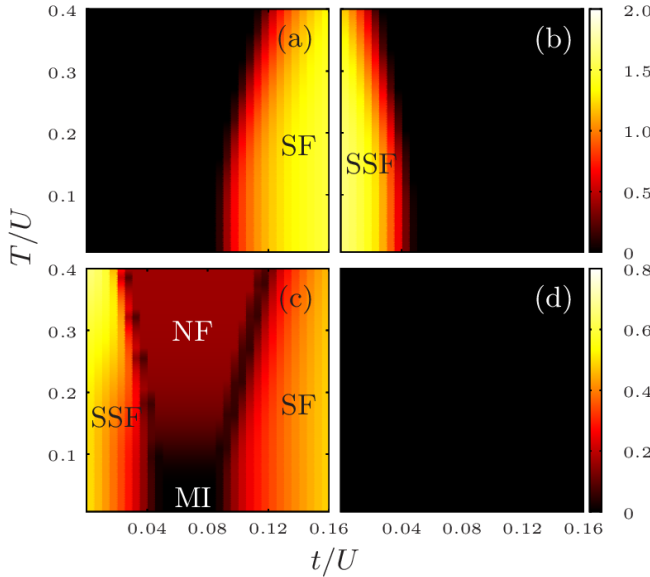


FIG. 2. The thermal-averaged Fourier transform of the single-particle correlation $M(\mathbf{k})$ at (a) $\mathbf{k} = (0, 0)$ and (b) $\mathbf{k} = (\pi, \pi)$, (c) compressibility κ , and (d) the structure factor $S(\pi, \pi)$ as a function of hopping and temperature at weak NN interaction $V = 0.24$. These are obtained using finite-temperature Gutzwiller mean-field theory in the grand-canonical ensemble. Here $\mu = 3.5$ is considered. Different kind of superfluidity is separated by MI at lower T and NF at higher T . Here, the maximum occupancy of bosons per site $n_{\max} = 10$ is assumed.

tries: the phase invariance of the superfluidity and translational invariance to form crystalline order [15, 16, 38, 66, 67]. These two broken symmetries result into a sharp peak of $M(\mathbf{k})$ at the center and four smaller peaks at finite \mathbf{k} in two-dimensional Brillouin zone, as shown in Fig. 1(b). Furthermore, the recent theoretical studies reported the presence of density-induced tunneling ($t' \neq 0$), at sufficiently higher densities leads to the existence of staggered superfluid (SSF) and staggered supersolid (SSS) phases [27–29]. The emergence of staggered quantum phases is attributed to the destructive interference between single-particle hopping and DIT. The momentum distributions $M(\mathbf{k})$ of the staggered phases reveal four sharp peaks at finite \mathbf{k} and $M(\pi, \pi) > M(0, 0)$ [Fig. 1(c,d)]. Here, we numerically determine the finite-temperature phase diagrams of isotropic dipolar bosons with correlated tunnelings. In particular, we choose higher average atomic density or chemical potential to examine the effects of DIT under the influence of thermal fluctuations.

In Fig. 2, we show the mean-field values of single-particle correlation $M(\mathbf{k})$, compressibility κ , and the structure factor $S(\pi, \pi)$ as a function of hopping and temperature. The truncation in the Fock space $n_{\max} = 10$ is chosen such that the phases reported in the present work do not depend on it. In our calculations, U sets the unit of energy scale, $U = 1$, and periodic boundary conditions are assumed. We first consider $\mu = 3.5$, $V = 0.24$ and $t' = -0.02$, where previous studies show the existence of the staggered quantum phases at $T = 0$ in square lattices [29]. In $T = 0$ limit, a MI(2) phase ap-

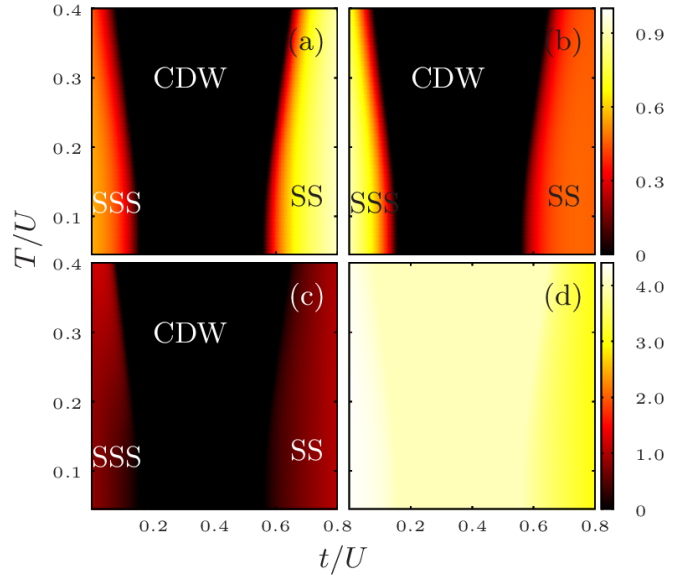


FIG. 3. Shown here are various observables at strong NN interaction ($V = 1$) in hopping (t) - temperature (T) plane. The upper panel shows the Fourier transform of the single-particle correlation $M(\mathbf{k})$ at (a) $\mathbf{k} = (0, 0)$ and (b) $\mathbf{k} = (\pi, \pi)$. In lower panel (c) the compressibility κ , and (d) structure factor at $\mathbf{k} = (\pi, \pi)$ are plotted. The chemical potential μ is chosen such that the effect of DIT introduces staggered phases. The normal and staggered supersolid phases are separated by incompressible CDW phase for the temperature limit considered. Here, the maximum occupancy per lattice site $n_{\max} = 10$.

pears in between two topologically distinct superfluid states. There exists a SSF phase for lower t , i.e. $t \sim |t'|$. This is confirmed by $M(0, 0) < M(\pi, \pi)$, finite compressibility, and zero density-density correlation [$S(\pi, \pi) = 0$]. However, at larger t , single-particle hopping driven normal superfluidity emerges. The thermal fluctuations melt both superfluid regions and widen the NF parameter space at higher temperatures, as expected. For lower hopping strengths, the value of $M(\pi, \pi)$ decreases with temperature which suggests a shrink in the novel staggered superfluidity regime [Fig. 2(b)]. We further present the finite-temperature phase diagram at higher off-site NN interaction, $V = 1$. It is pertinent to note that the DIT scales with NN interaction, hence we considered here $t' = -0.1$. The quantitative variations in the single-particle correlation $M(\mathbf{k})$ at $\mathbf{k}=(0, 0)$ [Fig. 3(a)] and (π, π) [Fig. 3(b)] suggest that the SSS phase is present at lower t and the normal SS phase at larger t . The two compressible phases are separated by a phase with zero correlations and compressibility [Fig. 3(c)] but finite structure factor $S(\pi, \pi) = 4$ [Fig. 3(d)]. This intervening phase is identified as CDW(4,0), which is also confirmed by the density contrast at two consecutive sites. As T increases, the CDW is robust to the thermal fluctuations and remains stable up to the maximum temperature range considered. However, at higher temperatures $T > 0.4$, we expect the incompressible CDW phase and compressible SS and SSS phases to melt into the normal fluid state.

In Fig. 4 we present the QMC results showing the typical

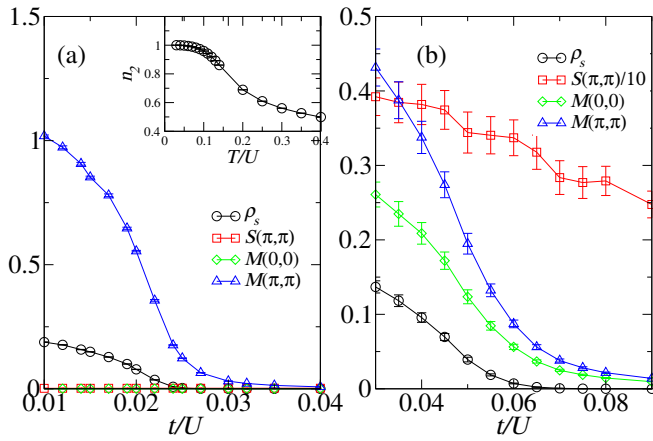


FIG. 4. The order parameters obtained by QMC as a function of t/U at $T/U = 0.2$ for (a) $V = 0.24$, $t' = -0.02$ and (b) $V = 1$, $t' = -0.1$, showing the SSF-NF and SSS-CDW phase transitions, respectively. The inset in (a) shows the crossover from MI(2) to NF as the double-occupancy n_2 decreases from its saturation value.

phase transitions of the SSF-NF (SSS-CDW) with $V = 0.24$ ($V = 1$) at finite temperature $T = 0.2$. Consistent with the Fig. 2 with small NN interaction $V = 0.24$ [Fig. 4(a)], single-particle correlation $M(\pi, \pi)$ is finite while $M(0, 0)$ vanishes at small t , which signals the SSF phase as the DIT (t') dominates the dynamics. When the domination of t' ends at $t \sim 0.025$, the superfluid coherence is destroyed and the system becomes a NF. Similarly, in the case of strong NN interaction $V = 1$ [Fig. 4(b)], the superfluidity order is destroyed as t/U increases, except now the diagonal long-range order remains intact, which indicates a continuous phase transition from SSS to CDW(4,0), again in agreement with the mean-field results shown in Fig. 3. Here, the staggered character of the supersolid phase is verified by $M(0, 0) < M(\pi, \pi)$.

Based on various observables using the mean-field and QMC simulations, we present the finite-temperature phase diagrams in Fig. 5. In the phase diagram for weak NN interaction [Fig. 5(a)], we find interesting features that the phase boundaries of the staggered superfluid and normal superfluid have opposite slopes on either side of the insulating (or NF) phase. It means when the single-particle hopping t increases, the critical temperature of SSF reduces to zero at a critical t and the system becomes a MI(2) solid. As t increases until another critical t , the normal SF stabilizes with its critical temperature increases with t . This opposite dependence of critical temperature on both sides of insulating regime on the hopping t can be understood by the competing role of t and t' . As shown in Eq. (8), the effective hopping of bosons depends on the occupation of neighboring sites and the competing values of t and t' . For the MI(2) phase, all sites are doubly occupied and the effective hopping vanishes if $t \sim -3t'$, i.e. near the middle of MI(2) phase with $t \sim 0.06$ in our case of weak NN interaction where $t' = -0.02$. For $t < 0.06$, the effective hopping becomes negative and results in SSF phase. The SSF phase, however, becomes less stable when t increases as the quantum coherence deteriorates, resulting in a lower crit-

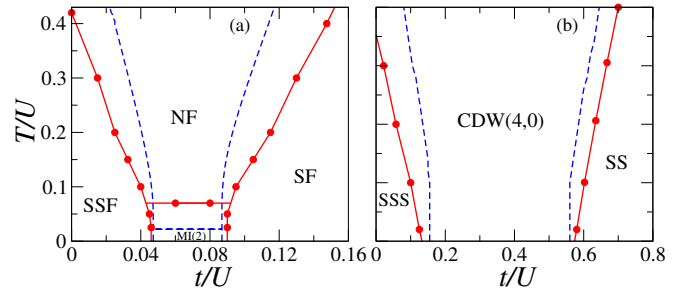


FIG. 5. The finite temperature phase diagram at $\mu = 3.5$ obtained using quantum Monte Carlo (solid lines) and Gutzwiller mean-field (dashed lines) approach. At finite temperatures, (a) for NN interaction comparable to the onsite interaction ($V = 0.24$), the compressible normal SF phase makes a transition to the SSF (as t decreases) with an intervening NF phase. (b) When V is strong ($V = 1$), a quantum phase transition between two types of supersolids occurs with an intervening CDW phase. The QMC corrects the prediction of the staggered phase regime using mean-field theory which overestimates the parameter space of compressible superfluid (supersolid) phases due to the poor resolution of atomic correlation between the lattice sites.

ical temperature. In contrast, when increasing $t > 0.06$ from the MI(2), the effective hopping is more positive and leads to a more stable SF and higher critical temperature. Therefore, the opposite dependence of the phase boundaries of SSF and SF on the hopping t is a clear demonstration of the interplay of the hopping terms t and t' . Similar mechanism also occurs for strong NN interaction [Fig. 5(b)] where $t' = -0.1$ and the zero effective hopping appears at $t \sim 0.3$, again near the middle of the insulating CDW(4,0) phase. The only difference here is that the strong interaction leads to the diagonal long-range ordering in the whole phase diagram and the CDW survives even in high temperature regime in the diagram and hence NF phase is not observed.

Although both the result of mean-field and QMC simulation provide the same feature of phase boundaries as mentioned above, there are quantitative differences between the two approaches. Previous studies have shown the importance of the QMC phase boundaries at finite temperatures [35, 45, 68]. The main difference can be seen in Fig. 5 is that the mean-field overestimates the staggered and normal superfluid regions due to poor intersite correlations. For example, at $\mu = 3.5$ the mean-field method shows SSF for $t = 0.03$ and $T = 0.3$, while the QMC predicts NF state. The critical hopping for the phase boundary separating SSF and NF obtained with QMC is lower and the deviations from the mean-field boundaries are prominent at higher temperatures. On the other hand, the critical value of t for NF-SF transition is larger for QMC. It is important to note that the mean-field theory predicts larger SSS and SS domains due to absence of inter-site atomic correlations, however these predictions are corrected by QMC calculations, cf. Fig. 5(b).

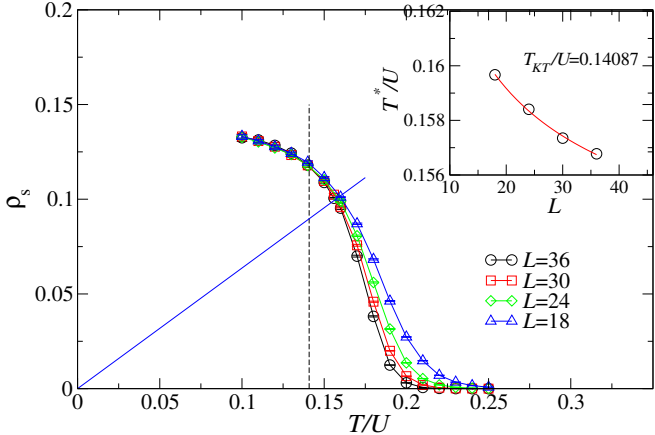


FIG. 6. Finite-size scaling of the superfluidity ρ_s as a function of T for $V = 0.24$, $t = 0.025$ and $\mu = 3.5$. The blue line represents the fitted T_{KT} . The blue line is $\rho_s = \frac{2}{\pi}T$, and its intersection with the $\rho_s(T)$ for various L gives $T^*(L)$, which shows excellent logarithmic dependence (inset) expected for KT transition (see the text).

IV. FINITE-SIZE SCALING ANALYSIS

A natural question arises about the thermal transition of staggered superfluid/supersolid to normal fluid/solid is whether it can be described by the Kosterlitz-Thouless transition as in the usual superfluid thermal phase transitions [69]. An instructive way to test the nature of the transition is via the finite-size scaling analysis, which we will describe here. In the thermodynamics limit, the superfluidity shows a universal jump at the KT transition temperature T_{KT} that $\rho_s(T_{\text{KT}}) = 2T_{\text{KT}}/\pi$ which, however, is subjected to a logarithmic correction $\rho_s(T_{\text{KT}}, L) = \rho_s(T_{\text{KT}}, \infty) \{1 + 1/[2 \ln(L/L_0)]\}$ for finite size L [70, 71]. The constant value L_0 and the transition temperature T_{KT} can be fitted by measuring the superfluidity of different system sizes L , as shown in Fig. 6. The temperatures T^* extracted from the interaction points $\rho_s(T^*) = \frac{2}{\pi}T^*$ for various system sizes L exhibit in a good agreement with the logarithmic correction $T^*(L) = T_{\text{KT}} \{1 + 1/[2 \ln(L/L_0)]\}$ (inset) expected for KT transition. In the normal SF, it is clear that the thermal fluctuations lead to the unbinding of vortex and anti-vortex pairs via the KT transition [72]. Our result suggests that the same mechanism is unaffected by shifting the condensation momentum from $(0,0)$ to (π, π) such that the staggered ordering of the superfluidity does not alter the nature of the thermal phase transition.

V. STAGGERED PHASES IN A TRAPPING POTENTIAL

We now consider the effects of realistic confinement on the staggered quantum phase transitions. The staggered phases result from the destructive interference between single-particle tunneling and DIT. In recent years, density-induced higher order processes have led to several novel phases, such as the interaction-driven mixing of orbitals [73] and correlated pair-tunneling leading to a twisted superfluid phase [74].

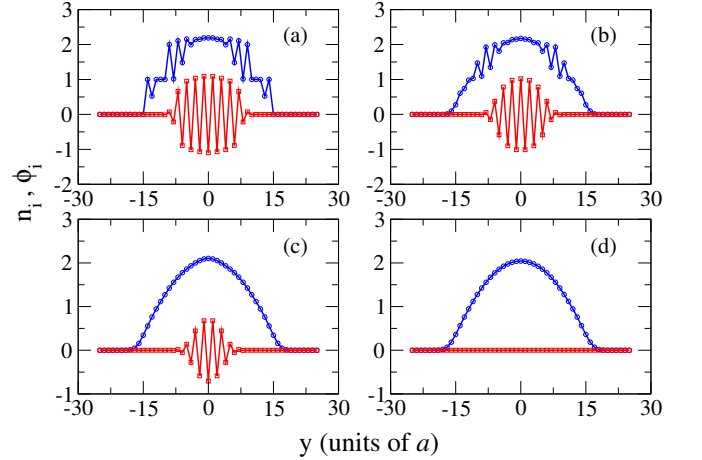


FIG. 7. The average number occupancy and SF order parameter for $L = 50$ square lattice along a one-dimensional cut at $x = 0$ within a confining potential. The density-distribution (blue circle) and order parameter (red square) profiles are shown for different temperatures (a) $T = 0.05$, (b) $T = 0.2$, (c) $T = 0.3$, (d) $T = 0.35$. With an increase in T , the staggered variations of ϕ_i reduces, which indicates a staggered-to-normal phase transition. The staggered quantum phases vanishes due to thermal fluctuations at $T \approx 0.35$. The other parameters chosen are $t = 0.025$, $\mu = 3.5$, $V = 0.24$, and temperatures are in units of U .

Here, we discuss the parameter regime which can provide the staggered quantum phases in the presence of a magneto-optical trap in cold-atom experiments. We add a spatially varying chemical potential to the offset energy term of the model Hamiltonian (1). The trapping potential is assumed as the harmonic potential $\epsilon_i = \Omega i^2$, with Ω sets the strength of the potential. In this external confinement the local chemical potential of the system changes as $\tilde{\mu} = \mu - \epsilon_i$. Co-existence of quantum phases occurs within the trapped system as a result of a change in $\tilde{\mu}$ within the trap. We have kept fixed the NN interaction $V = 0.24$, $\mu = 1$, and $\Omega = 0.015$. The latter ensures that the trapped atomic density vanishes at the edge of the lattice.

To illustrate the competition among different phases we have selected the cases $T = 0.05, 0.2, 0.3$ and 0.35 . Using the mean-field approach, we compute the local atomic distributions and the SF order parameter in the trap. We plot the density and order parameter profiles for $L = 50$ in Fig. 7. In particular, the plots are shown as a vertical cut at $x = 0$ of the trapped square lattice, to observe the effects of the trapping potential. First we start considering $T = 0.05$, where the observed effects are similar to the zero temperature case. From Fig. 7(a), we find a homogeneous atomic distribution (n_i) at the center of the trap while the SF order parameter modulates between the same number and an alternating sign. These properties characterize the SSF at the center of the trap. In addition, the SSF phase is surrounded by a density modulation with a staggered order parameter distribution indicating the parameter domain of SSS. It is important to note that the SS phase also exhibits modulations in n_i and ϕ_i but the variation in ϕ_i between two real numbers does not change sign. In

contrast, the staggered phase changes sign with the same (different) magnitude of the real numbers for SSF (SSS). Thus, the presence of harmonic potential exhibit the coexistence of two staggered quantum phases, SSF and SSS. At the edges of the trap, the superfluidity vanishes (as identified by $\phi_i = 0$) and the insulating (MI and CDW) or normal state surrounds the staggered phases.

We further show the effects of thermal fluctuations at finite temperatures on the stability of staggered phases. From Fig. 7(b) we observe the reduction in the regime with the modulation of ϕ_i at $T = 0.2$, however the constant density at the center and the crystalline nature of the phase near the trap center still persist. It shows that the melting of staggered quantum phases begins from the edges, and it is more pronounced at $T = 0.3$ [Fig. 7(c)]. At even higher temperatures, the staggered superfluidity vanishes and the normal fluid state occupies the trap due to the prevailing role of thermal fluctuations. The temperature corresponding to $T \approx 0.3$ is in the few-nK regime for the extended Bose-Hubbard model with DIT for ^{168}Er atoms [30]. Hence, the combined effects of the NN interaction as a genuine consequence of long-range interaction and interaction-driven DIT can lead to many-body staggered quantum phases in optical lattice experiments.

VI. CONCLUSION

We have studied the finite-temperature phase diagrams of soft-core dipolar bosons with density-induced tunneling in a square lattice potential. At weak dipolar interaction, the normal state intervenes between two topologically distinct su-

perfluid states while at strong interaction the staggered and normal supersolid phases appear on either side of the insulating density-wave solid state. Both the mean-field calculation and quantum Monte Carlo simulation show that the critical temperature of the staggered superfluid phase decreases with single-particle tunneling while that of the normal superfluid increases, which is resulting from the interplay of DIT and single-particle tunneling. We have further shown, by using finite-size scaling of superfluid density, that the thermal phase transition of staggered superfluidity is KT-type, just like that of normal superfluid. This result suggests that the staggering of the superfluid phase does not alter the symmetry breaking process of the off-diagonal long-range order. Finally, we reveal the coexistence of quantum phases in the presence of an external trapping potential at finite temperatures. In quantum gas experiments, thermal fluctuations play a decisive role in the emergence of quantum phases. Recent experimental advances in the observation of density-induced tunneling and the novel superfluidity and phase transitions discussed in the present work may provide a way to realize staggered superfluids in ultracold dipolar experiments.

ACKNOWLEDGMENTS

We thank M.-F. Yang and D. Angom for helpful discussions. K.S. acknowledges the support from IAMS, Academia Sinica and the Ministry of Science and Technology (MOST), Taiwan, under the Grant No. MOST-109-2112-M-001-035-MY3. K.-K. N. acknowledges the support by the National Science and Technology Council under Grant no. 110-2112-M-029 -004 and 111-2112-M-029 -007.

[1] M. Lewenstein, A. Sanpera, V. Ahufinger, B. Damski, A. Sen(De), and U. Sen, *Adv. Phys.* **56**, 243 (2007).

[2] I. Bloch, J. Dalibard, and W. Zwerger, *Rev. Mod. Phys.* **80**, 885 (2008).

[3] I. Bloch, J. Dalibard, and S. Nascimbène, *Nat. Phys.* **8**, 267 (2012).

[4] C. Gross and I. Bloch, *Science* **357**, 995 (2017).

[5] M. Greiner, O. Mandel, T. Esslinger, T. W. Hansch, and I. Bloch, *Nature (London)* **415**, 39 (2002).

[6] M. Aidelsburger, M. Atala, M. Lohse, J. T. Barreiro, B. Paredes, and I. Bloch, *Phys. Rev. Lett.* **111**, 185301 (2013).

[7] F. Schäfer, T. Fukuhara, S. Sugawa, Y. Takasu, and Y. Takahashi, *Nat. Rev. Phys.* **2**, 411 (2020).

[8] C. Chin, R. Grimm, P. Julienne, and E. Tiesinga, *Rev. Mod. Phys.* **82**, 1225 (2010).

[9] M. Aidelsburger, S. Nascimbene, and N. Goldman, *C. R. Physique* **19**, 394 (2018).

[10] D. M. Luz and R. R. dos Santos, *Phys. Rev. B* **54**, 1302 (1996).

[11] J. Hirsch, *Phys. C: Supercond. Appl.* **158**, 326 (1989).

[12] F. H. L. Essler, V. E. Korepin, and K. Schoutens, *Phys. Rev. Lett.* **68**, 2960 (1992).

[13] J. Appel, M. Grodzicki, and F. Paulsen, *Phys. Rev. B* **47**, 2812 (1993).

[14] I. Bloch, *Nat. Phys.* **1**, 23 (2005).

[15] T. Lahaye, C. Menotti, L. Santos, M. Lewenstein, and T. Pfau, *Rep. Prog. Phys.* **72**, 126401 (2009).

[16] M. A. Baranov, M. Dalmonte, G. Pupillo, and P. Zoller, *Chem. Rev.* **112**, 5012 (2012).

[17] M. J. Mark, E. Haller, K. Lauber, J. G. Danzl, A. J. Daley, and H.-C. Nägerl, *Phys. Rev. Lett.* **107**, 175301 (2011).

[18] D.-S. Lühmann, O. Jürgensen, and K. Sengstock, *New J. Phys.* **14**, 033021 (2012).

[19] S. Pilati and M. Troyer, *Phys. Rev. Lett.* **108**, 155301 (2012).

[20] S. Ospelkaus, C. Ospelkaus, O. Wille, M. Succo, P. Ernst, K. Sengstock, and K. Bongs, *Phys. Rev. Lett.* **96**, 180403 (2006).

[21] K. Günter, T. Stöferle, H. Moritz, M. Köhl, and T. Esslinger, *Phys. Rev. Lett.* **96**, 180402 (2006).

[22] T. Best, S. Will, U. Schneider, L. Hackermüller, D. van Oosten, I. Bloch, and D.-S. Lühmann, *Phys. Rev. Lett.* **102**, 030408 (2009).

[23] O. Jürgensen, K. Sengstock, and D.-S. Lühmann, *Phys. Rev. A* **86**, 043623 (2012).

[24] D.-S. Lühmann, K. Bongs, K. Sengstock, and D. Pfannkuche, *Phys. Rev. Lett.* **101**, 050402 (2008).

[25] O. Jürgensen, F. Meinert, M. J. Mark, H.-C. Nägerl, and D.-S. Lühmann, *Phys. Rev. Lett.* **113**, 193003 (2014).

[26] D.-S. Lühmann, *Phys. Rev. A* **94**, 011603 (2016).

[27] D. Johnstone, N. Westerberg, C. W. Duncan, and P. Öhberg, *Phys. Rev. A* **100**, 043614 (2019).

[28] R. Kraus, K. Biedroń, J. Zakrzewski, and G. Morigi, *Phys. Rev. B* **101**, 174505 (2020).

[29] K. Suthar, R. Kraus, H. Sable, D. Angom, G. Morigi, and J. Zakrzewski, *Phys. Rev. B* **102**, 214503 (2020).

[30] S. Baier, M. J. Mark, D. Petter, K. Aikawa, L. Chomaz, Z. Cai, M. Baranov, P. Zoller, and F. Ferlaino, *Science* **352**, 201 (2016).

[31] I. B. Spielman, W. D. Phillips, and J. V. Porto, *Phys. Rev. Lett.* **98**, 080404 (2007).

[32] B. Capogrosso-Sansone, i. m. c. G. m. c. Söyler, N. Prokof'ev, and B. Svistunov, *Phys. Rev. A* **77**, 015602 (2008).

[33] M. Rigol, G. G. Batrouni, V. G. Rousseau, and R. T. Scalettar, *Phys. Rev. A* **79**, 053605 (2009).

[34] K. Jiménez-García, R. L. Compton, Y.-J. Lin, W. D. Phillips, J. V. Porto, and I. B. Spielman, *Phys. Rev. Lett.* **105**, 110401 (2010).

[35] K. W. Mahmud, E. N. Duchon, Y. Kato, N. Kawashima, R. T. Scalettar, and N. Trivedi, *Phys. Rev. B* **84**, 054302 (2011).

[36] A. S. Sajna, T. P. Polak, R. Micnas, and P. Rożek, *Phys. Rev. A* **92**, 013602 (2015).

[37] M. O. C. Pires and E. J. V. de Passos, *Braz. J. Phys.* **47**, 1 (2017).

[38] K. Suthar, H. Sable, R. Bai, S. Bandyopadhyay, S. Pal, and D. Angom, *Phys. Rev. A* **102**, 013320 (2020).

[39] R. Bai, D. Gaur, H. Sable, S. Bandyopadhyay, K. Suthar, and D. Angom, *Phys. Rev. A* **102**, 043309 (2020).

[40] H.-J. Chen, Y.-Q. Yu, D.-C. Zheng, and R. Liao, *Sci. Rep.* **10**, 9076 (2020).

[41] G. Ceccarelli and C. Torrero, *Phys. Rev. A* **85**, 053637 (2012).

[42] M. Gupta, H. R. Krishnamurthy, and J. K. Freericks, *Phys. Rev. A* **88**, 053636 (2013).

[43] R. Landig, L. Hruba, N. Dogra, M. Landini, R. Mottl, T. Donner, and T. Esslinger, *Nature (London)* **532**, 476 (2016).

[44] C. Lagoin, U. Bhattacharya, T. Grass, R. Chhajlany, T. Salamon, K. Baldwin, L. Pfeiffer, M. Lewenstein, M. Holzmann, and F. Dubin, “Checkerboard solid of dipolar excitons in a two-dimensional lattice,” (2022), arXiv:2201.03311 [cond-mat.str-el].

[45] L. de Forges de Parny, F. Hébert, V. G. Rousseau, and G. G. Batrouni, *Eur. Phys. J. B* **85**, 169 (2012).

[46] L. de Forges de Parny and V. G. Rousseau, *Phys. Rev. A* **95**, 013606 (2017).

[47] M. C. Gutzwiller, *Phys. Rev. Lett.* **10**, 159 (1963).

[48] D. S. Rokhsar and B. G. Kotliar, *Phys. Rev. B* **44**, 10328 (1991).

[49] W. Krauth, M. Caffarel, and J.-P. Bouchaud, *Phys. Rev. B* **45**, 3137 (1992).

[50] K. Sheshadri, H. R. Krishnamurthy, R. Pandit, and T. V. Ramakrishnan, *EPL* **22**, 257 (1993).

[51] R. Bai, S. Bandyopadhyay, S. Pal, K. Suthar, and D. Angom, *Phys. Rev. A* **98**, 023606 (2018).

[52] K. V. Krutitsky, *Phys. Rep.* **607**, 1 (2016).

[53] S. Pal, R. Bai, S. Bandyopadhyay, K. Suthar, and D. Angom, *Phys. Rev. A* **99**, 053610 (2019).

[54] K. Suthar, P. Kaur, S. Gautam, and D. Angom, *Phys. Rev. A* **104**, 043320 (2021).

[55] P. Buonsante and A. Vezzani, *Phys. Rev. A* **70**, 033608 (2004).

[56] L. Pollet, *Rep. Prog. Phys.* **75**, 094501 (2012).

[57] A. W. Sandvik, *Phys. Rev. B* **59**, R14157 (1999).

[58] O. F. Syljuåsen and A. W. Sandvik, *Phys. Rev. E* **66**, 046701 (2002).

[59] A. Dorneich and M. Troyer, *Phys. Rev. E* **64**, 066701 (2001).

[60] M. P. A. Fisher, P. B. Weichman, G. Grinstein, and D. S. Fisher, *Phys. Rev. B* **40**, 546 (1989).

[61] D. Jaksch, C. Bruder, J. I. Cirac, C. W. Gardiner, and P. Zoller, *Phys. Rev. Lett.* **81**, 3108 (1998).

[62] F. Gerbier, *Phys. Rev. Lett.* **99**, 120405 (2007).

[63] K.-K. Ng, *Phys. Rev. B* **82**, 184505 (2010).

[64] K.-K. Ng and M.-F. Yang, *Phys. Rev. B* **83**, 100511 (2011).

[65] D.-S. Lühmann, *Phys. Rev. A* **87**, 043619 (2013).

[66] K.-K. Ng and Y.-C. Chen, *Phys. Rev. B* **77**, 052506 (2008).

[67] S. Bandyopadhyay, R. Bai, S. Pal, K. Suthar, R. Nath, and D. Angom, *Phys. Rev. A* **100**, 053623 (2019).

[68] T. Flottat, L. d. deParny, F. Hébert, V. G. Rousseau, and G. G. Batrouni, *Phys. Rev. B* **95**, 144501 (2017).

[69] G. Schmid, S. Todo, M. Troyer, and A. Dorneich, *Phys. Rev. Lett.* **88**, 167208 (2002).

[70] H. Weber and P. Minnhagen, *Phys. Rev. B* **37**, 5986 (1988).

[71] Y.-D. Hsieh, Y.-J. Kao, and A. W. Sandvik, *J. Stat. Mech.: Theory Exp.* **2013**, P09001 (2013).

[72] J. M. Kosterlitz and D. J. Thouless, *J. Phys. C: Solid State Phys.* **6**, 1181 (1973).

[73] P. Soltan-Panahi, D.-S. Lühmann, J. Struck, P. Windpassinger, and K. Sengstock, *Nat. Phys.* **8**, 71 (2012).

[74] O. Jürgensen, K. Sengstock, and D.-S. Lühmann, *Sci. Rep.* **5**, 12912 (2015).